Nano Materials Science 5 (2023) 78–85

Contents lists available at ScienceDirect

Nano Materials Science

journal homepage: www.keaipublishing.com/cn/journals/nano-materials-science/

Stable yellow light emission from lead-free copper halides single crystals for visible light communication

Baiqian Wang [a], Yuru Tang [b], Xin Yang [a], Wensi Cai [a], Ru Li [a], Wen Ma [a], Shuangyi Zhao [a,*], Chen Chen [b,**], Zhigang Zang [a,***]

[a] Key Laboratory of Optoelectronic Technology & Systems (Ministry of Education), Chongqing University, Chongqing, 400044, China
[b] School of Microelectronics and Communication Engineering, Chongqing University, Chongqing, 400044, China

ARTICLE INFO

Keywords:
Lead-free copper halides
Single crystals
Yellow light-emitting diodes
Visible light communication (VLC)

ABSTRACT

Yellow light-emitting diodes (LEDs) as soft light have attracted abundant attention in lithography room, museum and art gallery. However, the development of efficient yellow LEDs lags behind green and blue LEDs, and the available perovskites yellow LEDs suffer from the instability. Herein, a pressure-assisted cooling method is proposed to grow lead-free $CsCu_2I_3$ single crystals, which possess uniform surface morphology and enhanced photoluminescence quantum yield (PLQY) stability, with only 10% PLQY losses after being stored in air after 5000 h. Then, the single crystals used for yellow LEDs without encapsulation exhibit a decent Correlated Color Temperature (CCT) of 4290 K, a Commission Internationale de l'Eclairage (CIE) coordinate of (0.38, 0.41), and an excellent 570-h operating stability under heating temperature of 100 °C. Finally, the yellow LEDs facilitate the application in wireless visible light communication (VLC), which show a −3 dB bandwidth of 21.5 MHz and a high achievable data rate of 219.2 Mbps by using orthogonal frequency division multiplexing (OFDM) modulation with adaptive bit loading. The present work not only promotes the development of lead-free single crystals, but also inspires the potential of $CsCu_2I_3$ in the field of yellow illumination and wireless VLC.

1. Introduction

Metal halide perovskites have attracted numerous attention as promising next-generation light emitters due to their great optoelectronic properties such as tunable emission spectra, high photoluminescence quantum yield (PLQY), exceptional defect tolerance, low cost and low temperature synthesis process [1–5]. Therefore, red [6–10], green [11–15] and blue [16–20] light-emitting diodes (LEDs) based on perovskites have shown high luminance and broad color gamut. In fact, there is a key spectrum ozone of yellow light with wavelength range from 577 to 597 nm. The yellow light is regarded as an important component in white emission, which may decide the final color rendering index (CRI) in solid-state-lighting and display [21–23]. Besides, the yellow light with lower radiant energy is seemed as a "soft" light source, which plays a key role in several special occasions, including lithography room, museum, art gallery and traffic indicator. In these fields, the yellow light facilitates to prevent the naked eyes and photosensitive collection from strong-light injures. As a result, the yellow light can be regarded as an ideal luminance source, which may not only compensate the spectrum loss in commercial screen, but also enhance the CRI values of white light [24]. However, the development of high-performance yellow LEDs lags behind these of green and blue LEDs.

Recently, perovskites also have been reported to exhibit excellent yellow emission, but the poor chemical and optical stability may severely limit their practical application [25]. It is found that $CsPbX_3$ (X = Cl, Br, I) perovskites with mixed halogens possess intrinsic yellow emission, which may be used to act as yellow emitters in yellow LEDs [13]. Zeng et al. designed yellow LEDs based on $CsPb(Br/I)_3$ quantum dots, which might emit a 586 nm yellow light with a full width at half maxima (FWHM) of 23 nm [26]. However, owing to the phase transition and separation of $CsPb(Br/I)_3$ with high molar ratio of iodine, the yellow emission cannot maintain for long time. Du et al. incorporated manganese ions (Mn^{2+}) into $CsPb(Cl/Br)_3$ quantum dots with high PLQY [27], because of the energy transfer from perovskite to Mn^{2+} and radiative

* Corresponding author.
** Corresponding author.
*** Corresponding author.
E-mail addresses: shyzhao@cqu.edu.cn (S. Zhao), c.chen@cqu.edu.cn (C. Chen), zangzg@cqu.edu.cn (Z. Zang).

https://doi.org/10.1016/j.nanoms.2022.03.003
Received 5 January 2022; Accepted 25 February 2022
Available online 1 April 2022

recombination between the energy levels of Mn^{2+}. The yellow LEDs based on the Mn^{2+}-doped $CsPb(Cl/Br)_3$ quantum dots showed a CRI value of 74, correlated color temperature (CCT) of 3459 K, and a Commission Internationale de L'Eclairage (CIE) chromaticity coordinate (0.42, 0.41). Although the above reported yellow perovskites LEDs show an improved performance, their poor stability and toxicity are the challenges for the commercial application.

In light of toxicity of Pb, substitution of Pb with other element (Mn, Fe, Cu, Zn, Ag, Sn, Sb) is expected to be a better choice. The lead-free $(C_6H_{18}N_2)SnBr_6(CH_3OH)$ with a peak wavelength of 590 nm and a FWHM of 127 nm, was pioneered by Ning et al. [28]. But the organic groups of hybrid perovskites may suffer from separation and degradation at high temperature, leading to unsatisfied stability. Recently, $CsCu_2I_3$ powders and thin films were reported as the excellent yellow light emitters by Guo et al. [29] and Shan et al. [30]. However, the poor half-lifetime (~5 h, h) and low luminance (<50 cd/m^2) hinder its further application. Generally, single crystals with few charge traps possess superior optoelectronic properties, which have promising potential in high-performance optoelectronic devices, compared to their corresponding polycrystalline films [31]. Hence, it is necessary to prepare high-quality single crystals with few defects and low surface energy [32].

In this work, a facile pressure-assisted cooling method is proposed to prepare lead-free $CsCu_2I_3$ single crystals. Compared with the reported ones, the as-prepared $CsCu_2I_3$ single crystals possess larger sizes and lower surface defect density, which are due to the controlled crystalline growth benefiting from the pressure provided from the autoclave. The optimum $CsCu_2I_3$ single crystals show a yellow photoluminescence with a peak wavelength of 580 nm and a large FWHM of 122 nm, which is owing to the mechanism of self-trapped excitons (STEs). In addition, after being stored at atmosphere for 5000 h, the PLQY of single crystals prepared by the pressure-assisted cooling method only reduced to 90% of their initial value, implying the enhanced chemical and optical stability. Thus, yellow LEDs were fabricated by exciting the $CsCu_2I_3$ single crystals by ultraviolet (UV) chips, which show a CRI of 78, a CCT of 4290 K and an CIE coordinate of (0.38, 0.41). Due to the good stability of the single crystals, the yellow LEDs exhibit a well-operated performance when continuously driven in air at 100 °C. The yellow LEDs with efficient and stable properties may not only act as a promising solid-state lighting source, but also be employed as emitters in wireless visible light communication (VLC). In a wireless VLC system with the yellow LEDs, it is found that a −3 dB bandwidth is 21.5 MHz, and an achievable data rate are obtained by orthogonal frequency division multiplexing (OFDM) modulation is 219.2 Mbps, exhibiting a prominent potential in the application of wireless VLC. Therefore, our work about $CsCu_2I_3$ single crystals may suggest their potential applications in both luminance for special occasions and wireless VLC, promoting the development of lead-free perovskite yellow LEDs.

2. Results and discussion

Fig. 1a indicates one-dimensional (1D) crystal structure of $CsCu_2I_3$, which belongs to orthorhombic space group of *Cmcm* [33]. The basic

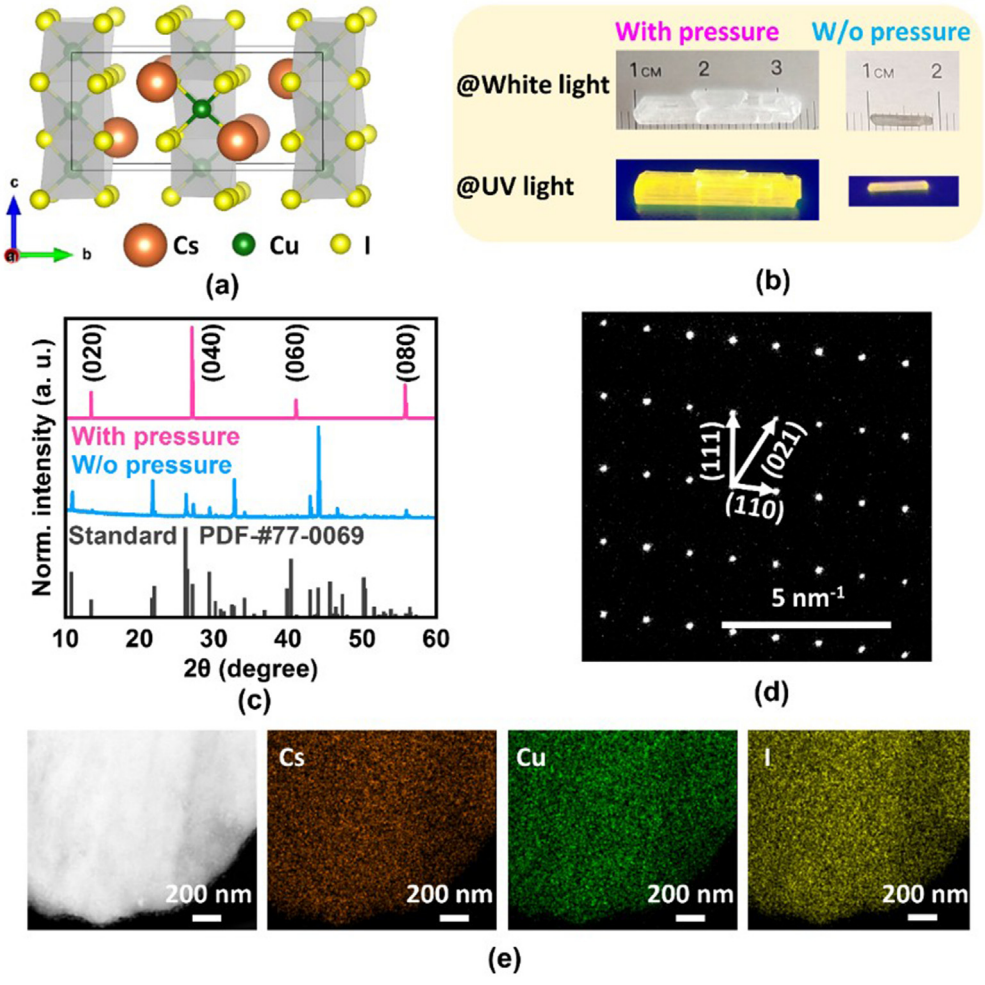

Fig. 1. (a) Crystal structures diagram of $CsCu_2I_3$. (b) Photographs and (c) XRD of grown $CsCu_2I_3$ single crystals without and with pressure. (d) Electron diffraction pattern and (e) Cs, Cu, I elemental mapping images of $CsCu_2I_3$ single crystals growth with pressure.

units of $CsCu_2I_3$ are edge-shared $[CuI_4]^{3-}$tetrahedras, which are isolated by Cs^+, forming a 1D chain-like architecture [34]. 1D perovskite crystals with well-defined crystal structures and unique one-dimensional closed surfaces have emerged as new material systems for optoelectronic device applications, which are expected to play a significant role as building blocks for next-generation optoelectronic devices [35]. Fig. 1b presents photographs of as-synthesized $CsCu_2I_3$ single crystals grown with and without pressure under white-light and UV-excitation. Compared with the single crystal grown with conventional method, the as-prepared single crystal grown with pressure-assisted strategy possesses a larger size of 2.3 cm as well as rod-like sharp and smooth surface morphology. The large size and smooth surface morphology of the $CsCu_2I_3$ single crystal can be attributed to their excellent crystallinity from the pressure-assisted cooling strategy employed in this work (The method grew single crystals without and with pressure in experimental section). Besides, the crystal phase of the grown single crystals was investigated by X-ray diffraction (XRD) patterns, in which the XRD patterns coincide well with their standard XRD patterns (Fig. 1c). The $CsCu_2I_3$ single crystals grown with pressure exhibit fewer number of peaks and extremely narrow FWHM of 0.06° on (020) crystal plane, which indicates the crystallinity is better than that of growth without pressure. During the preparation process, the high pressure in autoclave may boost the saturated vapor pressure of the precursor solution, promoting the solubility of precursor. In addition, the controlled cooling processing may enhance the crystallinity and orientation of the single crystals [36], which has been confirmed by the clear crystal lattices and electron diffraction pattern, as shown in Fig. 1d. The electron diffraction result can reveal that the crystal system of the $CsCu_2I_3$ single crystals belongs to an orthorhombic group [37]. Fig. 1e shows the elemental mapping characterization of the single crystals grown with pressure, where the uniform distribution of cesium (Cs), copper (Cu) and iodine (I) has been found, indicating the negligible aggregation and phase separation of the $CsCu_2I_3$ single crystals. Moreover, energy dispersive spectrometer (EDS) mapping and scanning electron microscopy (SEM) images of $CsCu_2I_3$ single crystals grown with pressure were characterized, and the results were shown in Table S1 and Fig. S1, respectively. The real elemental ratio of Cs, Cu and I is close to the ideal one of 1: 2: 3, and the elemental states were characterized by X-ray photoelectron spectroscopy (XPS) (Fig. S2). It is confirmed that the chemical components of the as-prepared single crystals consist of Cs^+, Cu^+ and I^- without oxidation, implying their chemical stability in air [38].

As shown in Fig. 2a, the $CsCu_2I_3$ single crystals grown by the two methods exhibit the similar photoluminescence (PL) spectra with peaks at 580 nm. Importantly, the pressure facilitates to enhance the PLQY of single crystals from 11.8% to 17.7% (Fig. S3). The PLQY of $CsCu_2I_3$ single crystals is up to 17.7%, which is the higher performance for reported $CsCu_2I_3$ perovskites [38–42]. Besides, the PL decay time of the $CsCu_2I_3$ single crystals grown with pressure is found to change from non-radiative time (τ_1) of 61.18 ns and radiative time (τ_2) of 431.37 ns toτ_1 of 60.39 ns andτ_2 of 489.71 ns (Fig. 2b and Table S2), implying the increase of radiative recombination rates induced by the passivation of defects[43]. The corresponding recombination time (τ_1 andτ_2) is longer than these of the lead halide perovskites[44], suggesting that phonons participate in the light-emitting process to extend the decay time. In addition, benefiting from the excellent crystallinity and surface morphology of single crystals, the PL mapping of the $CsCu_2I_3$ single crystals grown with pressure collected under a 325 nm pump excitation with an area of 0.04 mm^2 exhibited the uniform yellow emission (Fig. 2c). It is a proof for high quality of single crystals, facilitating the application of the $CsCu_2I_3$ single crystals with yellow emission. The absorption (Abs.), photoluminescence excitation (PLE) and PL spectra of $CsCu_2I_3$ single crystals grown with pressure are shown in Fig. 2d. The PLE peak locating at 337 nm may correspond to the exciton absorption of $CsCu_2I_3$ single crystals. The PL spectrum exhibits a peak of 580 nm and a FWHM of 122 nm, indicating a yellow broad emission of the single crystals. Fig. 2e and **f** shows emission-wavelength dependent PLE spectra and excitation-wavelength dependent PL spectra. No shift is found for PLE and PL spectra, but their intensity may change under various exciting and detecting wavelength, indicating the emission energy levels of $CsCu_2I_3$ are unchanged. Moreover, a large Stokes shift (~243 nm), which is defined as the

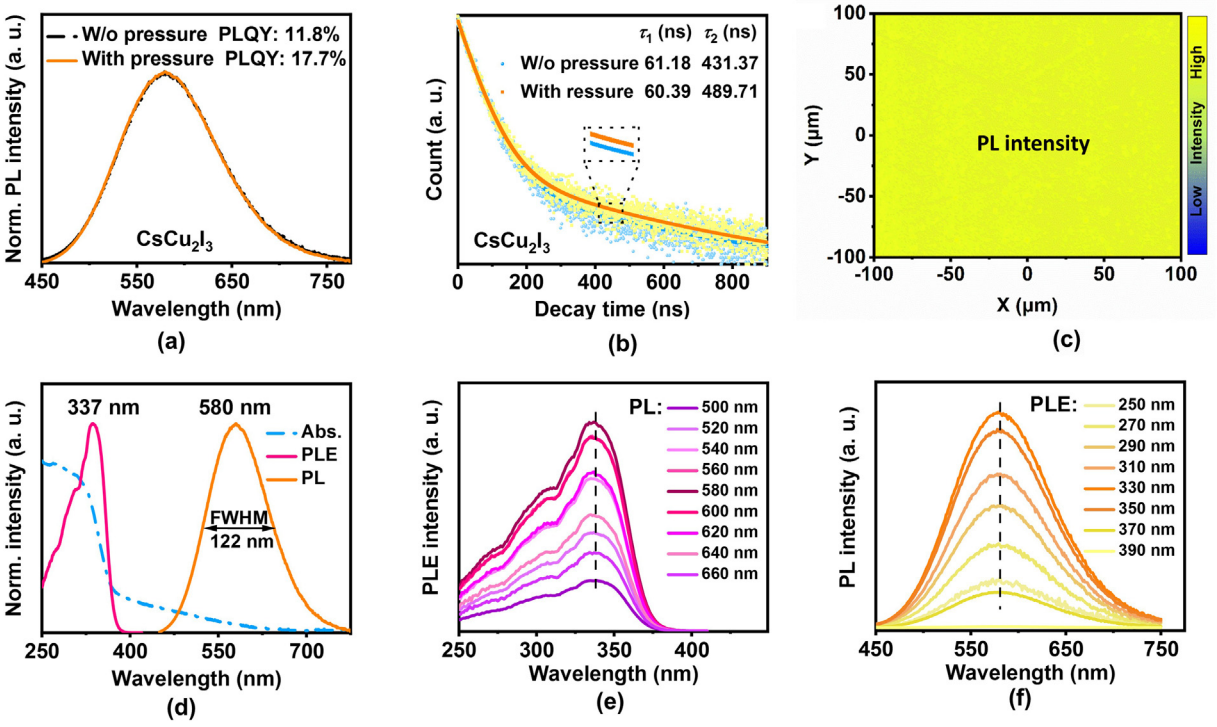

Fig. 2. (a) Photoluminescence (PL) and (b) Transient PL decay time of $CsCu_2I_3$ single crystals grown without and with pressure. (c) PL mapping excited by 325 nm laser. (d) Absorption (abs.), photoluminescence excitation (PLE) and PL, (e) Emission-wavelength dependent PLE spectra and (f) Excitation-wavelength dependent PL spectra of grown $CsCu_2I_3$ single crystals with pressure.

difference between PLE and PL peaks, is similar with that in lead-free Sn-based perovskites[45], implying that the PL mechanism of $CsCu_2I_3$ single crystal may be STEs instead of band-edge emission. Furthermore, we measured the Raman spectra of as-grown $CsCu_2I_3$ single crystals to determine their longitudinal optical phonon energies, as can be seen in Fig. S4. The Stokes Raman spectra are dominated by the modes at 120 cm^{-1}, which is assigned to the vibration of I–Cu–I[46]. The soft 1D structure of $CsCu_2I_3$ may deform under the light excitation, in which the distorted $[CuI_4]^{3-}$ tetrahedras can lead to the presence of STEs[47]. As a result, the excited excitons would transfer from the excited level to the STEs energy level, followed by the radiative recombination between STEs and ground energy level. Thus, the novel yellow broadband emission with the large Stokes shift and higher PLQY occur in $CsCu_2I_3$ single crystals grown with pressure.

To evaluate the suitability of as-synthesized $CsCu_2I_3$ single crystals grown with pressure for practical applications, we investigated the effects of heat, polar solvent, and environmental oxygen/moisture on the structure and optical properties of $CsCu_2I_3$ single crystals. Firstly, the successive heating/cooling cycling tests were conducted in the temperature range from 25 to 100 °C, and the integrated PL intensity at heating and cooling temperature point was plotted in Fig. 3a. The PL intensity at 25 °C is higher than that of 100 °C, which is due to the temperature-induced fluorescent quenching [48]. It is worth noting that the emission degradation of the single crystals at high temperature is almost recoverable after cooling them to room temperature, and the final PL spectrum are unchanged (Fig. 3b). To further explore the temperature tolerance of $CsCu_2I_3$ single crystals, the thermogravimetric (TG) curve was performed to study the change of the single crystals at high temperature. As shown in Fig. 3c, when the testing temperature enhances to 500 °C, the weight of the single crystals doesn't change. However, due to the thermal sublimation of $CsCu_2I_3$ single crystals at higher temperature, the obvious changes occur when the crystals are furtherly heated to 800 °C. It is found the evaporation T_{05} (T_{05} is defined as the temperature at which the weighting loss is 5 wt%), T_{10}, T_{50}, and T_{90} are 591, 619, 702, 759 °C, respectively. Such a high changing temperature can ensure its application in a variety of fields. Secondly, we investigated the polar-solvent tolerance of $CsCu_2I_3$ single crystals, including deionized water, methanol, ethanol, and isopropanol (Fig. S5). After being soaked in these solvents for 5 h, when excited under UV light (365 nm), the $CsCu_2I_3$ single crystal in isopropanol with less polarity exhibited bright yellow emission, while the $CsCu_2I_3$ single crystal in the water showed red emission from original yellow PL. It is due to that the polarity of water is very larger than that of isopropanol, which decomposes $CsCu_2I_3$ into CsI and CuI. As a result, CsI is dissolved in water, but the insoluble CuI is coating in $CsCu_2I_3$ may be seemed as the origin of the red emission under UV light. Apart from the prominent optical performance, the long-term stability of the single crystals was investigated by measure their PLQY in Fig. 3d. It is found that their PLQY values are maintained 90% of the initial value over 5000 h stored in air, suggesting the excellent optical stability of inorganic lead-free $CsCu_2I_3$ single crystals. Finally, after storing the $CsCu_2I_3$ single crystal in air for 5000 h, their XRD results showed that no new peaks were observed, indicating the negligible decomposition and oxidation of the single crystals (Fig. S6).

To study the optoelectronic applications of the inorganic lead-free $CsCu_2I_3$ single crystals grown with pressure, yellow LEDs were prepared via simple pasting the $CsCu_2I_3$ single crystals on 365 nm UV chips. When applying various driving voltages onto the yellow LEDs, the corresponding electroluminescence (EL) spectra are collected. As shown in Fig. 4a, the EL intensity enhances with the increase of driving voltages, while the peaks of EL spectra are not found to change. Apart from the EL intensity, the luminance of the yellow LEDs may enhances when increasing applied voltages, reaching to a maximum luminance of 14340 cd/m^2 at 3.6 V (Fig. 4b). However, when further boosting the driving voltages, the luminance of the yellow LEDs didn't enhance, which is attributed to the thermal quenching from the surged temperature of UV chips under high operating voltages. Thus, the yellow LEDs operating at a

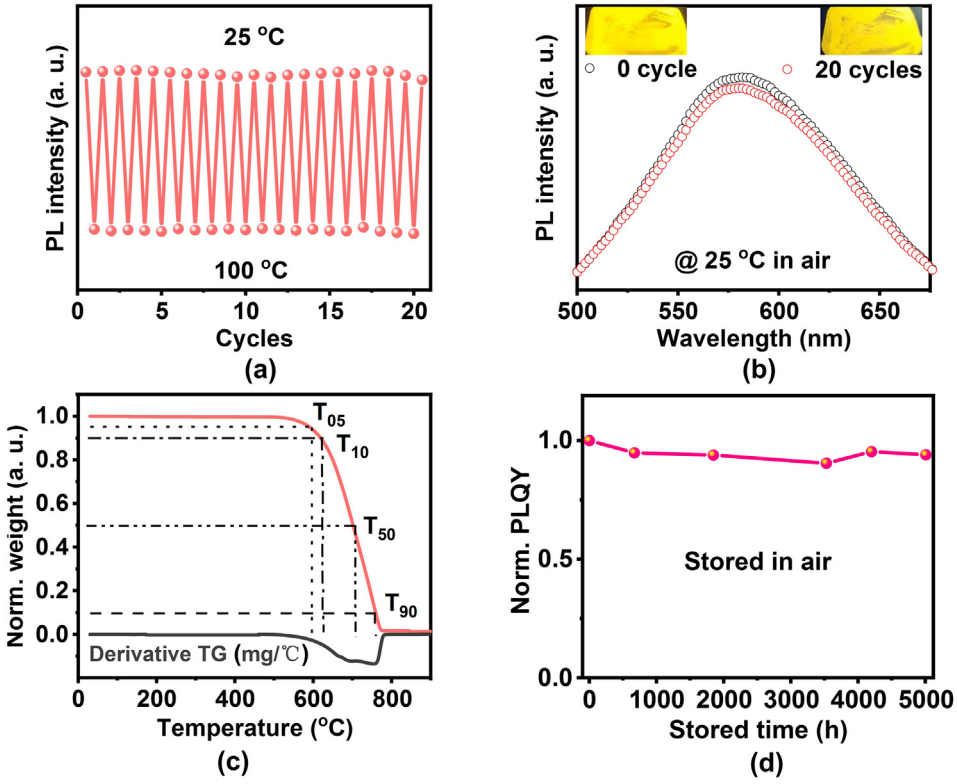

Fig. 3. (a) 20 heating/cooling cycling tests of $CsCu_2I_3$ single crystals at two representative temperature points (25 and 100 °C). (b) Corresponding PL spectra of $CsCu_2I_3$ single crystals before and after heating/cooling cycling. The inset photograph is a $CsCu_2I_3$ single crystal before and after heating/cooling cycling under UV 365 nm. (c) Thermogravimetric (TG) curves of $CsCu_2I_3$ single crystals. (d) Variety of PLQY of $CsCu_2I_3$ single crystals stored in air.

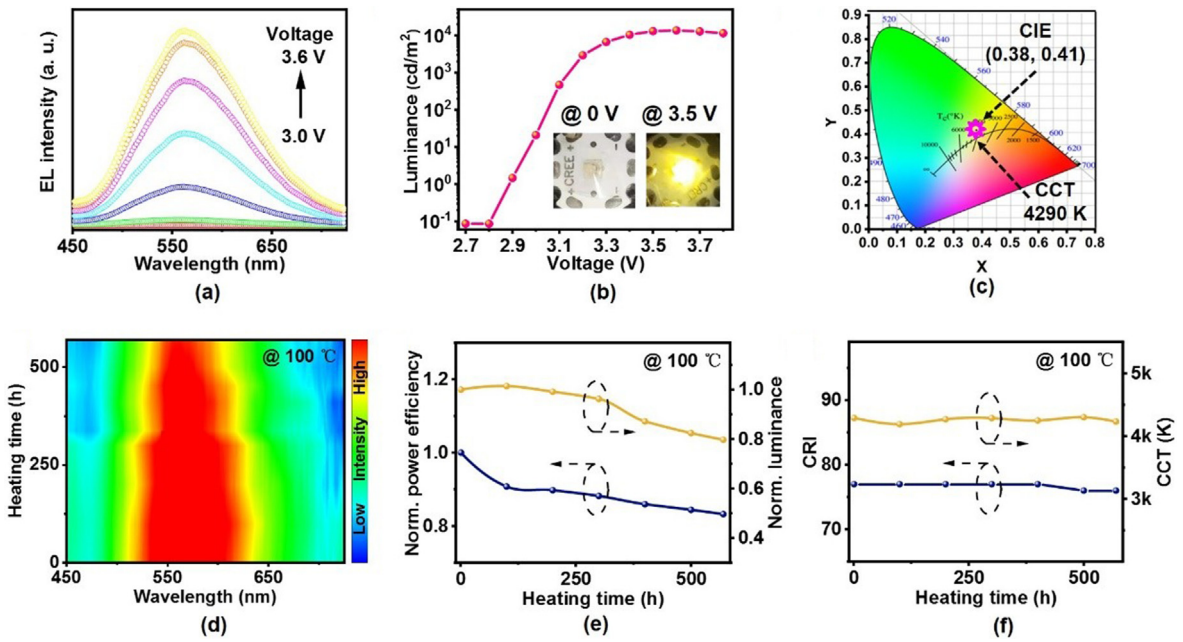

Fig. 4. (a) EL spectra under different driving voltages of as-prepared yellow LEDs with $CsCu_2I_3$ single crystals. (b) Luminance-voltage curves of the yellow LEDs. (c) CIE chromaticity diagram of the prepared yellow LEDs. (d) Contour mapping of the EL spectra, (e) Changes of normalized power efficiency and luminance, (f) Evolution of CRI and CCT of yellow LED during the 570-h operation at 100 °C.

driving voltage of 3.5 V exhibit an emissive performance including a CIE color coordinate of (0.38, 0.41), a CRI of 78 and a decent CCT of 4290 K (Fig. 4c). The external quantum efficiency of the yellow LEDs based on the photoluminescence is shown in Fig. S7. Furthermore, the yellow LEDs were tested on a 100 °C hotplate in air to study their long-term stability. As shown in Fig. 4d and **e**, the EL spectra of the yellow LEDs didn't shift, and their power efficiency and luminance are found to maintain almost 80% of their initial values after 570 h operation. Furthermore, the negligible changes of the CRI and CCT of the yellow LEDs over 570 h can illustrate their ultrahigh operating stability, implying the application potential of the yellow LEDs (Fig. 4f). This excellent stability of the devices is benefit from the good tolerance of heat, polar solvent, environmental oxygen/moisture, and light (Fig. 3). Obviously, this device has advantage in operation stability in Table S3.

Owing to the efficient and stable performance of the yellow LEDs, they can be employed as light sources in a wireless VLC system. As shown in Fig. 5a, we explored the communication performance of the yellow LEDs employed as the light source in an experimental wireless VLC system, which consists of the yellow light source, a signal generator, a photodetector and a driver. The light source is modulated by the output signal of the signal generator and emits optical signal, which is seemed as the information for communication. Fig. 5b presents the electrical-optical-electrical (EOE) frequency response of the wireless VLC system using the proposed yellow LEDs under a DC bias of 3.5 V. Apparently, the wireless VLC system exhibits a typical low-pass frequency response, which possesses a -3dB bandwidth of ~21.5 MHz, which is greater than those of down-conversion LEDs (<2 MHz)[11,14,49]. The inset in Fig. 5b shows the captured eye diagram from a square wave at a frequency of 22 MHz, which is clear and wide-open. Fig. 5c shows the received signal-to-noise ratio (SNR) performance with a modulation bandwidth of 62 MHz, in which the gradual reduction of the SNR is found with the increase of the frequency. As shown in Fig. 5d, the bit loading profile exhibits a similar decrease with the increase of the frequency. The corresponding received constellation diagrams are plotted in Fig. 5e, which include binary phase shift keying (BPSK), 4-ary quadrature amplitude modulation (4QAM), 8QAM, 16QAM, 32QAM and 64QAM constellations. In order to further improve the EOE frequency response of the wireless VLC system using the yellow LEDs, OFDM modulation with adaptive bit loading can be adopted to fully explore achievable data rate of the system. The achievable data rate of the OFDM modulation is obtained by the equation of $R = Blog_2(M)$[50]. Where B is the modulation bandwidth of the OFDM signal and M is the achievable maximum QAM constellation. By applying OFDM modulation with adaptive bit loading, the maximum achievable rate of the system is calculated to be 219.2 Mbps.

3. Conclusion

In this work, we adopted a pressure-assisted cooling method to prepare $CsCu_2I_3$ single crystals, which exhibit large sizes, uniform orientations and smooth surfaces, facilitating the enhanced optical performance and stability against air and heat. Their broad PL spectrum with a peak at 580 nm are exhibited, which possesses a PLQY of 17.7% and a large Stokes (243 nm). The all mentioned optical properties of the $CsCu_2I_3$ single crystal are attributed to the STE mechanism, implying feasibility for preparation of yellow LEDs. The resulted yellow LEDs exhibited a decent CCT of 4290 K, and an excellent CIE coordinate of (0.38, 0.41), as well as an ultra-stable operation at high temperatures in air. In addition, the yellow LEDs serve as the light sources of wireless VLC systems, in which a -3dB bandwidth of 21.5 MHz and a high data rate of 219.2 Mbps can be achieved, indicating the promising potentials of $CsCu_2I_3$ single crystal in various optoelectronic applications.

4. Experimental section

4.1. Materials

Cesium iodide (CsI, 99.9%) and Hydroiodic acid (HI, 45–50%) were purchased from Aladdin Chemistry Technology Co., Ltd. Cuprous iodide (CuI, 99.9%) and Hypophoaphoeous acid (H_3PO_2, 50%) were purchased from Macklin Inc.

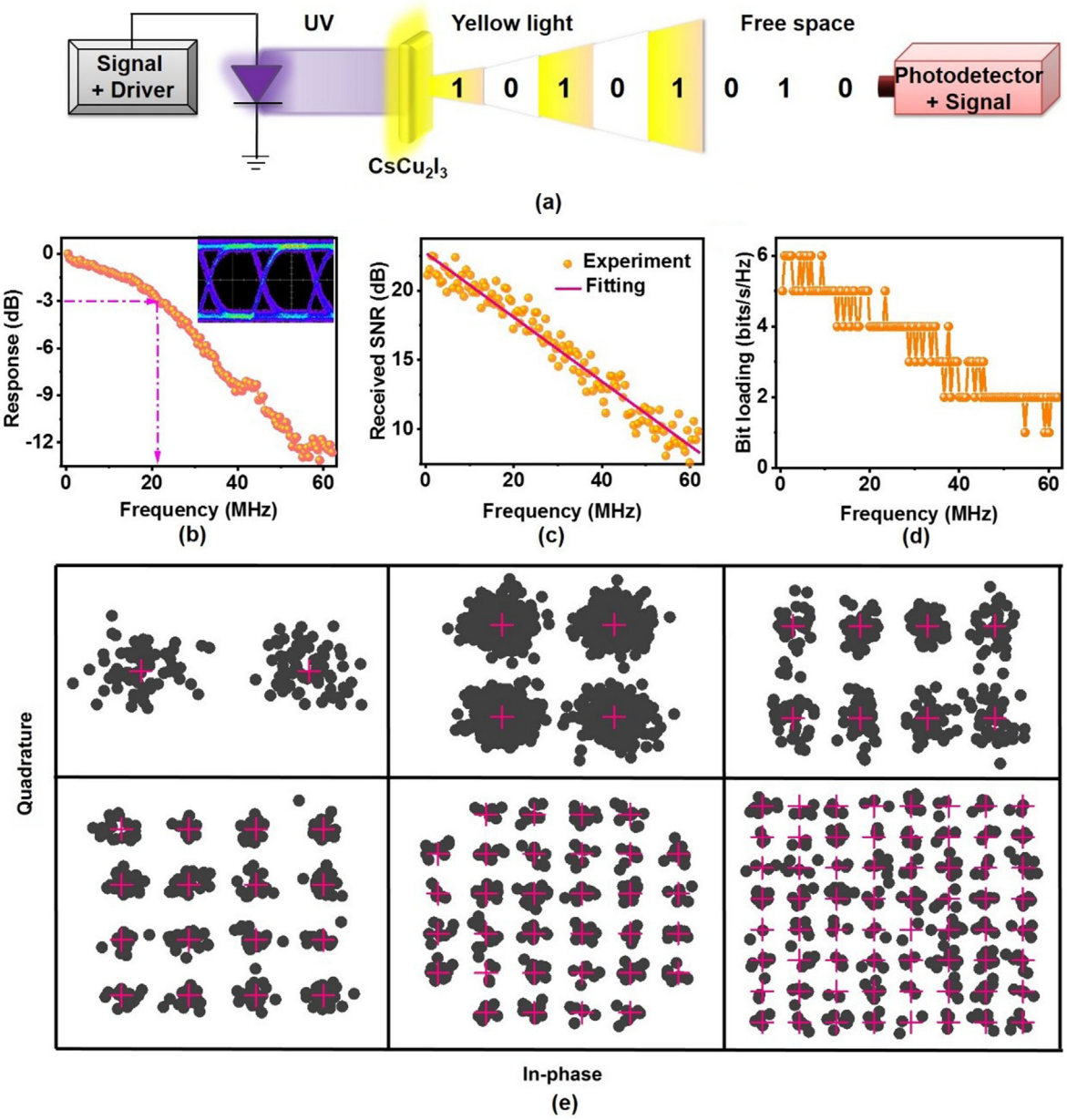

Fig. 5. (a) Schematic diagram of the wireless VLC system using the yellow LEDs, (b) EOE frequency response of the system with the inset showing the captured eye diagram, (c) Received SNR, (d) bit loading profile of the wireless VLC system using OFDM modulation, and (e) Corresponding constellation diagrams of binary phase shift keying (BPSK), 4QAM, 8QAM, 16QAM, 32QAM and 64QAM, respectively.

4.2. Crystal growth

CsI (1.298 g, 5 mmol), CuI (1.904 g, 10 mmol), HI (20 ml), H_3PO_2 (0.6 ml) and Magneton were added to a glass bottle. The mixture was stirred at 100 °C for 3 h. Next, the white precipitate was removed by Polytetrafluoroethylene (PTFE 0.45 μm) filters and syringes, and the saturated solution was injected into the PTFE lining of the autoclave. This autoclave was placed in a heating table with 100 °C and kept for 3 h. And then, the autoclave was cooled to room temperature by 1 °C/h. Finally, $CsCu_2I_3$ single crystals were obtained after filtering, washing and finally vacuum dried.

The container of the cooling method without pressure is ordinary glass bottle, while that of the cooling method with pressure is PTFE lining of the autoclave. The heating table (JW-400) was purchased from Wuhan Junwei Technology Company.

4.3. Material characterization

The TEM images and EDS results collected from Talos F200S (ThermoFisher Scientific, Netherlands). The SEM images was collected with a tungsten filament scanning electron microscope Phenom ProX (ThermoFisher Scientific, Netherlands). The XRD results were collected by a PANalytical X' Pert Powder (Spectris Pte. Ltd, Netherlands) with a Cu Kα tube operated at 40 kV and 40 mA. The XPS was measured by ESCALAB250Xi (Thermo Fisher Scientific. USA). The Thermogravimetric and differential scanning calorimeter (TG-DSC) data was implemented on a TGA2 (Mettler Toledo, Switzerland). All the PLE/PL/PLQY/τ were measured by FLS1000 (Edinburgh Instruments, England).

4.4. Preparation and measurement of light-emitting diodes (LEDs)

All LEDs were prepared by paste the single crystal on commercial UV

chips (365 nm) with glue. The Electro-optical characteristics of LEDs, including Voltage-Luminance, Electroluminescent (EL) spectra, CIE (x,y) coordinates, CRI, CCT and Deviation of devices were measured and recorded by a computer-controlled sourcemeter (Keithley 2400, USA) and a spectrascan (PR-670, USA). The AC signal generated by an arbitrary waveform generator (Rigol DG4102, China), was combined with 3.5 V DC bias via a bias-T (Mini-Circuits Bias-Tee ZFBT-6GW+, USA), and the output signal was loaded into the LEDs. Photodetector (Hamamatsu C12702-12, Japan) with a -3dB bandwidth of 62 MHz was employed to convert photoelectric signals, and the resultant electrical signal was recorded by a digital storage oscilloscope (LeCroy WaveSurfer 432, USA).

Supporting Information

Supporting Information is available from the website of journal or from the author.

Declaration of competing interest

The authors declare no conflict of interest.

Acknowledgements

This work is funded by National Natural Science Foundation of China (Nos. 61904023, 11974063); Fundamental Research Funds for the Central Universities (2021CDJQY-022); Natural Science Foundation of Chongqing (No. cstc2019jcyj-bshX0078, cstc2020jcyj-jqX0028). The authors would like to thank Shijuan Xiao and Chuanyao Yang at Analytical and Testing Center of Chongqing University for their assistance with XRD and PL analysis.

Appendix A. Supplementary data

Supplementary data to this article can be found online at https://doi.org/10.1016/j.nanoms.2022.03.003.

References

[1] D.D. Yan, S.Y. Zhao, Y.B. Zhang, H.X. Wang, Z.G. Zang, Highly efficient emission and high-CRI warm white light-emitting diodes from ligand-modified $CsPbBr_3$ quantum dots, Opto-Electron Adv. 5 (2022) 200075.
[2] Y.C. Liu, Z. Xu, Z. Yang, Y.X. Zhang, J. Cui, Y.H. He, H.C. Ye, K. Zhao, H.M. Sun, R. Lu, M. Liu, M.G. Kanatzidis, S.Z. Liu, Inch-size 0D-structured lead-free perovskite single crystals for highly sensitive stable X-ray imaging, Matter 3 (1) (2020) 1–17.
[3] S.Y. Zhao, Y.B. Zhang, Z.G. Zang, Room-temperature doping of ytterbium into efficient near-infrared emission $CsPbBr_{1.5}Cl_{1.5}$ perovskite quantum dots, Chem. Commun. 56 (43) (2020) 5811–5814.
[4] W.S. Cai, H.Y. Li, M.C. Li, M. Wang, H.X. Wang, J.Z. Chen, Z.G. Zang, Opportunities and challenges of inorganic perovskites in high-performance photodetectors, J. Phys. D Appl. Phys. 54 (2021) 293002.
[5] X.Z. Xu, W. Deng, X.J. Zhang, L.M. Huang, W. Wang, R.F. Jia, D. Wu, X.H. Zhang, J.S. Jie, S.T. Lee, Dual-band, high-performance phototransistors from hybrid perovskite and organic crystal array for secure communication applications, ACS Nano 13 (5) (2019) 5910–5919.
[6] C.H. Liu, E. Hamzehpoor, Y. Sakai-Otsuka, T. Jadhav, D.F. Perepichka, A pure-red doublet emission with 90% quantum yield: stable, colorless, iodinated triphenylmethane solid, Angew. Chem. Int. Ed. 59 (2020) 23030–23034.
[7] B. Jeong, H. Han, Y.J. Choi, S.H. Cho, E.H. Kim, S.W. Lee, J.S. Kim, C. Park, D. Kim, C. Park, All-inorganic $CsPbI_3$ perovskite phase-stabilized by poly(ethylene oxide) for red-light-emitting diodes, Adv. Funct. Mater. 28 (2018) 1706401.
[8] J. Pan, Y. Shang, J. Yin, M. De Bastiani, W. Peng, I. Dursun, L. Sinatra, A.M. El-Zohry, M.N. Hedhili, A.H. Emwas, O.F. Mohammed, Z. Ning, O.M. Bakr, Bidentate ligand-passivated $CsPbI_3$ perovskite nanocrystals for stable near-unity photoluminescence quantum yield and efficient red light-emitting diodes, J. Am. Chem. Soc. 140 (2) (2018) 562–565.
[9] G.H. Huang, G.C. Xie, J.H. Wang, C.B. Jiang, C.H. Mai, Y. Luo, J. Wang, J.B. Peng, Y. Cao, A strategy for improving the performance of perovskite red light-emitting diodes by controlling the growth of perovskite crystal, J. Mater. Chem. C 7 (38) (2019) 11887–11895.
[10] H. Wang, Y. Dou, P. Shen, L. Kong, H. Yuan, Y. Luo, X. Zhang, X. Yang, Molecule-induced p-doping in perovskite nanocrystals enables efficient color-saturated red light-emitting diodes, Small 16 (20) (2020) 2001062.
[11] X.W. Li, W.S. Cai, H.L. Guan, S.Y. Zhao, S.L. Cao, C. Chen, M. Liu, Z.G. Zang, Highly stable $CsPbBr_3$ quantum dots by silica-coating and ligand modification for white light-emitting diodes and visible light communication, Chem. Eng. J. 419 (2021) 129551.
[12] Z.M. Chen, Z.C. Li, Z. Chen, R.X. Xia, G.R.X. Zou, L.H. Chu, S.J. Su, J.B. Peng, H.L. Yip, Y. Cao, Utilization of trapped optical modes for white perovskite light-emitting diodes with efficiency over 12%, Joule 5 (2) (2021) 456–466.
[13] W. Feng, K. Lin, W. Li, X. Xiao, J. Lu, C. Yan, X. Liu, L. Xie, C. Tian, D. Wu, K. Wang, Z. Wei, Efficient all-inorganic perovskite light-emitting diodes enabled by manipulating the crystal orientation, J. Mater. Chem. 9 (17) (2021) 11064–11072.
[14] S.Y. Zhao, C. Chen, W.S. Cai, R. Li, H.Y. Li, S.Q. Jiang, M. Liu, Z.G. Zang, Efficiently luminescent and stable lead-free $Cs_3Cu_2Cl_5$@silica nanocrystals for white light-emitting diodes and communication, Adv. Opt. Mater. 9 (13) (2021) 2100307.
[15] H.L. Guan, S.Y. Zhao, H.X. Wang, D.D. Yan, M. Wang, Z.G. Zang, Room temperature synthesis of stable single silica-coated $CsPbBr_3$ quantum dots combining tunable red emission of Ag-In-Zn-S for high-CRI white light-emitting diodes, Nano Energy 67 (2020) 104279.
[16] J. Zhang, Y. Yang, H. Deng, U. Farooq, X.K. Yang, J. Khan, J. Tang, H.S. Song, High quantum yield blue emission from lead-free inorganic antimony halide perovskite colloidal quantum dots, ACS Nano 11 (9) (2017) 9294–9302.
[17] S.C. Hou, M.K. Gangishetty, Q.M. Quan, D.N. Congreve, Efficient blue and white perovskite light-emitting diodes via manganese doping, Joule 2 (2018) 1–13.
[18] Z.C. Li, Z.M. Chen, Y.C. Yang, Q.F. Xue, H.L. Yip, Y. Cao, Modulation of recombination zone position for quasi-two-dimensional blue perovskite light-emitting diodes with efficiency exceeding 5%, Nat. Commun. 10 (2019) 1027.
[19] Y.T. Dong, M.J. Choi, Y. Hou, Y.K. Wang, B. Chen, F.L. Yuan, M.J. Wu, S. Lee, H. Ebe, P. Todorovic, F. Dinic, A. Johnston, M. Chekini, S.W. Baek, B. Sun, P.C. Li, S. Hoogland, H.T. Kung, E. Kumacheva, E. Spiecker, L.S. Liao, Z.H. Lu, E.H. Sargent, Bipolar-shell resurfacing for blue LEDs based on strongly confined perovskite quantum dots, Nat. Nanotechnol. 15 (2020) 668–674.
[20] S.Y. Zhao, Q.H. Mo, W.S. Cai, H.X. Wang, Z.G. Zang, Inorganic lead-free cesium copper chlorine nanocrystal for highly efficient and stable warm white light-emitting diodes, Photon. Res. 9 (2) (2021) 187–192.
[21] L.J. Wang, Z.Q. Kou, B.Q. Wang, J. Zhou, Z.Y.C. Lu, L.X. Li, Realizing high efficiency/CRI/color stability in the hybrid white organic light emitting diode by manipulating exciton energy transfer, Opt. Mater. 115 (2021) 111059.
[22] J. Zhou, Z.Q. Kou, L.J. Wang, B.Q. Wang, X. Chen, X. Sun, Z.X. Zheng, Realizing high-performance color-tunable WOLED by adjusting the recombination zone and energy distribution in the emitting layer, J. Phys. D Appl. Phys. 54 (2021) 265107.
[23] B.Q. Wang, Z.Q. Kou, Q.S. Yuan, X.E. Fu, Z.T. Fan, A. Zhou, Improving CRI of white phosphorescence organic light-emitting diodes by controlling exciton energy transfer in the planar heterojunction, Org. Electron. 78 (2020) 105617.
[24] B.Q. Wang, Z.Q. Kou, Y. Tang, F.Y. Yang, X.E. Fu, Q.S. Yuan, High CRI and stable spectra white organic light-emitting diodes with double doped blue emission layers and multiple ultrathin phosphorescent emission layers by adjusting the thickness of spacer layer, Org. Electron. 70 (2019) 149–154.
[25] X.M. Li, J.X. Chen, D.D. Yang, X. Chen, D.L. Geng, L.F. Jiang, Y. Wu, C.F. Meng, H.B. Zeng, $Mn^{(2+)}$ induced significant improvement and robust stability of radioluminescence in $Cs_3Cu_2I_5$ for high-performance nuclear battery, Nat. Commun. 12 (1) (2021) 3879.
[26] J.Z. Song, J.H. Li, X.M. Li, L.M. Xu, Y.H. Dong, H.B. Zeng, Quantum dot light-emitting diodes based on inorganic perovskite cesium lead halides ($CsPbX_3$), Adv. Mater. 27 (44) (2015) 7162–7167.
[27] W.W. Chen, X.S. Tang, Z.G. Zang, Y. Shi, Z.Q. Yang, J. Du, Tunable dual emission in $Mn^{(2+)}$-doped $CsPbX_3$ (X = Cl, Br) quantum dots for high efficiency white light-emitting diodes, Nanotechnology 30 (7) (2019), 075704.
[28] P.F. Fu, M.L. Huang, Y.Q. Shang, N. Yu, H.L. Zhou, Y.B. Zhang, S.Y. Chen, J.K. Gong, Z.J. Ning, Organic-inorganic layered and hollow tin bromide perovskite with tunable broadband emission, ACS Appl. Mater. Interfaces 10 (40) (2018) 34363–34369.
[29] N. Liu, X. Zhao, M.L. Xia, G.D. Niu, Q.X. Guo, L. Gao, J. Tang, Light-emitting diodes based on all-inorganic copper halide perovskite with self-trapped excitons, J. Semiconduct. 41 (5) (2020), 052204.
[30] Z.Z. Ma, Z.F. Shi, C.C. Qin, M.H. Cui, D.W. Yang, X.J. Wang, L.T. Wang, X.Z. Ji, X.C. Chen, J.L. Sun, D. Wu, Y. Zhang, X.J. Li, L.J. Zhang, C.X. Shan, Stable yellow light-emitting devices based on ternary copper halides with broadband emissive self-trapped excitons, ACS Nano 14 (4) (2020) 4475–4486.
[31] W. Deng, J.S. Jie, X.Z. Xu, Y.L. Xiao, B. Lu, X.J. Zhang, X.H. Zhang, A microchannel-confined crystallization strategy enables blade coating of perovskite single crystal arrays for device integration, Adv. Mater. 32 (16) (2020) 1908340.
[32] S.Y. Zhao, W.S. Cai, H.X. Wang, Z.G. Zang, J.Z. Chen, All-inorganic lead-free perovskite(-like) single crystals: synthesis, properties, and applications, Small Methods 5 (2021) 2001308.
[33] S.L. Cheng, A. Beitlerova, R. Kucerkova, E. Mihokova, M. Nikl, Z.Y. Zhou, G.H. Ren, Y.T. Wu, Non-hygroscopic, self-absorption free, and efficient 1D $CsCu_2I_3$ perovskite single crystal for radiation detection, ACS Appl. Mater. Interfaces 13 (10) (2021) 12198–12202.
[34] P.F. Cheng, L. Sun, L. Feng, S.Q. Yang, Y. Yang, D.Y. Zheng, Y. Zhao, Y.B. Sang, R.L. Zhang, D.H. Wei, W.Q. Deng, K.L. Han, Colloidal synthesis and optical properties of all-inorganic low-dimensional cesium copper halide nanocrystals, Angew. Chem. Int. Ed. 58 (45) (2019) 16087–16091.
[35] X.Z. Xu, X.J. Zhang, W. Deng, J.S. Jie, X.H. Zhang, 1D organic inorganic hybrid perovskite micro nanocrystals fabrication assembly and optoelectronic application, Small Methods 2 (2018) 1700340.
[36] Q.H. Mo, C. Chen, W.S. Cai, S.Y. Zhao, D.D. Yan, Z.G. Zang, Room Temperature Synthesis of Stable Zirconia-Coated $CsPbBr_3$ Nanocrystals for White Light-Emitting Diodes and Visible Light Communication, Laser Photonics. Rev. 15 (10) (2021) 2100278, https://doi.org/10.1002/lpor.202100278.

[37] X.M. Mo, T. Li, F.C. Huang, Z.X. Li, Y.L. Zhou, T. Lin, Y.F. Ouyang, X.M. Tao, C.F. Pan, Highly-efficient all-inorganic lead-free 1D $CsCu_2I_3$ single crystal for white-light emitting diodes and UV photodetection, Nano Energy 81 (2021) 105570.
[38] S.F. Fang, Y. Wang, H.X. Li, F.E. Fang, K. Jiang, Z.X. Liu, H.N. Li, Y.M. Shi, Rapid synthesis and mechanochemical reactions of cesium copper halides for convenient chromaticity tuning and efficient white light emission, J. Mater. Chem. C 8 (14) (2020) 4895–4901.
[39] R.C. Lin, Q.L. Guo, Q. Zhu, Y.M. Zhu, W. Zheng, F. Huang, All-Inorganic $CsCu_2I_3$ single crystal with high-PLQY (approximately 15.7%) intrinsic white-light emission via strongly localized 1D excitonic recombination, Adv. Mater. 31 (46) (2019) 1905079.
[40] M.Y. Zhang, J.S. Zhu, B. Yang, G.D. Niu, H.D. Wu, X. Zhao, L.X. Yin, T. Jin, X.Y. Liang, J. Tang, Oriented-structured $CsCu_2I_3$ film by close-space sublimation and nanoscale seed screening for high-resolution X-ray imaging, Nano Lett 21 (3) (2021) 1392–1399.
[41] P. Vashishtha, G.V. Nutan, B.E. Griffith, Y.N. Fang, D. Giovanni, M. Jagadeeswararao, T.C. Sum, N. Mathews, S.G. Mhaisalkar, J.V. Hanna, T. White, Cesium copper Iodide tailored nanoplates and nanorods for blue, yellow, and white emission, Chem. Mater. 31 (21) (2019) 9003–9011.
[42] R.C. Lin, Q. Zhu, Q.L. Guo, Y.M. Zhu, W. Zheng, F. Huang, Dual self-trapped exciton emission with ultrahigh photoluminescence quantum yield in $CsCu_2I_3$ and $Cs_3Cu_2I_5$ perovskite single crystals, J. Phys. Chem. C 124 (37) (2020) 20469–20476.
[43] J.Y. Di, J.J. Chang, S.Z. Liu, Recent progress of two-dimensional lead halide perovskite single crystals: crystal growth, physical properties, and device applications, EcoMat 2 (3) (2020) 1–24.
[44] Q.H. Mo, T.C. Shi, W.S. Cai, S.Y. Zhao, D.D. Yan, J. Du, Z.G. Zang, Room temperature synthesis of stable silica-coated $CsPbBr_3$ quantum dots for amplified spontaneous emission, Photon. Res. 8 (2020) 1605–1612.
[45] Y. Yu, Z.D. An, X.Y. Cai, M.L. Guo, C.B. Jing, Y.Q. Li, Recent progress of tin-based perovskites and their applications in light-emitting diodes, Acta Phys. Sin. 70 (4) (2021), 048503.
[46] J.J. Luo, X.M. Wang, S.R. Li, J. Liu, Y.M. Guo, G.D. Niu, L. Yao, Y.H. Fu, L. Gao, Q.S. Dong, C.Y. Zhao, M.Y. Leng, F.S. Ma, W.X. Liang, L.D. Wang, S.Y. Jin, J.B. Han, L.J. Zhang, J. Etheridge, J.B. Wang, Y.F. Yan, E.H. Sargent, J. Tang, Efficient and stable emission of warm-white light from lead-free halide double perovskites, Nature 563 (7732) (2018) 541–545.
[47] M.H. Du, Emission trend of multiple self-trapped excitons in luminescent 1D Copper halides, ACS Energy Lett 5 (2) (2020) 464–469.
[48] Z.Z. Ma, Z.F. Shi, D.W. Yang, Y.W. Li, F. Zhang, L.T. Wang, X. Chen, D. Wu, Y.T. Tian, Y. Zhang, L.J. Zhang, X.J. Li, C.X. Shan, High color-rendering index and stable white light-emitting diodes by assembling two broadband emissive self-trapped excitons, Adv. Mater. 33 (2) (2021) 2001367.
[49] W. Deng, X.C. Jin, Y. Lv, X.J. Zhang, X.H. Zhang, J.S. Jie, 2D ruddlesden-popper perovskite nanoplate based deep-blue light-emitting diodes for light communication, Adv. Funct. Mater. 29 (40) (2019) 1903861.
[50] B.Q. Wang, C. Chen, X. Yang, W.S. Cai, S.Y. Zhao, R. Li, W. Ma, J.Z. Chen, Z.G. Zang, Pressure-assisted cooling to grow ultra-stable $Cs_3Cu_2I_5$ and $CsCu_2I_3$ single crystals for solid-state lighting and visible light communication, EcoMat 4 (2022) 12184.